ELSEVIER

Spectrochimica Acta Part B 61 (2006) 1091 – 1097

SPECTROCHIMICA ACTA PART B

www.elsevier.com/locate/sab

Automated nanoliter solution deposition for total reflection X-ray fluorescence analysis of semiconductor samples ☆

Chris M. Sparks [a,*], Carolyn H. Gondran [a], George J. Havrilla [b], Elizabeth P. Hastings [b]

[a] *Process Characterization Laboratory, ATDF, Austin, TX 78741, United States*
[b] *Chemistry Division, Los Alamos National Laboratory, Los Alamos, NM 87545, United States*

Received 9 December 2005; accepted 15 September 2006
Available online 7 November 2006

Abstract

In this study, a BioDot BioJet dispensing system was investigated as a nanoliter sample deposition method for total reflection X-ray fluorescence (TXRF) analysis. The BioDot system was programmed to dispense arrays of 20 nL droplets of sample solution on Si wafers. Each 20 nL droplet was approximately 100 μm in diameter. A 10 × 10 array (100 droplets) was deposited and dried in less than 2 min at room temperature and pressure, demonstrating the efficiency of the automated deposition method. Solutions of various concentrations of Ni and Ni in different matrices were made from stock trace element standards to investigate of the effect of the matrix on the TXRF signal. The concentrations were such that the levels of TXRF signal saturation could be examined. Arrays were deposited to demonstrate the capability of drying 100 μL of vapor phase decomposition-like residue in the area of a typical TXRF detector.
© 2006 Elsevier B.V. All rights reserved.

Keywords: Total reflection X-ray fluorescence; TXRF; Vapor phase decomposition; VPD; Nanoliter dried spot deposition

1. Introduction

In the semiconductor industry, the need to control metallic contamination on silicon wafers in high risk areas (for example, pre-gate dielectric cleans) requires a technique with detection limits in the E08 atoms/cm^2 range [1]. A sample preconcentration step like vapor phase decomposition (VPD) combined with total reflection X-ray fluorescence spectroscopy (TXRF) for analyzing the dried VPD residue can achieve these low detection limits [2–4]. The VPD process involves exposing the wafer to hydrofluoric acid vapor which etches the silicon dioxide layer, native or thermal, leaving a hydrophobic silicon surface. A collection solution, from 50–200 μL, is then scanned across the wafer gathering the metallic contamination into a single droplet. The solution could then be quantitatively analyzed for metals by inductively coupled plasma-mass spectrometry (ICP-MS) or dried as a residue on the wafer and analyzed by TXRF. While the VPD-TXRF technique is well established in the semiconductor industry, there are some potential drawbacks that need to be addressed. Recent reports in the literature suggest that saturation of the TXRF signal can under-report the true value of the contamination in analyses where the contamination in the residue is greater than 3 ng [5,6], thus limiting the linear dynamic range of the technique. It has also been shown that control of the effects of the dried VPD residue's morphology on the TXRF signal is of critical importance affecting reproducibility and accuracy when matching a sample to a standard [7–11]. The advances in nanoliter quantity dispensing instrumentation that include rapid droplet drying time [12] and programmable dispensing patterns make it worth investigating as a novel approach for drying VPD residue on the wafer to improve the accuracy and precision of VPD-TXRF measurements.

2. Experimental

Arrays of solution were deposited with a BioDot BioJet AD 3050 (Irving, CA) deposition system onto a 200 mm bare Si

☆ This paper was presented at the 11th International Conference on Total Reflection X-ray Fluorescence Spectrometry and Related Methods (TXRF 2005) held in Budapest, Hungary, 18–22 September 2005, and is published in the special issue of Spectrochimica Acta Part B, dedicated to that conference.

* Corresponding author. Tel.: +1 512 356 3030; fax: +1 512 356 7008.
E-mail address: chris.sparks@atdf.com (C.M. Sparks).

0584-8547/$ - see front matter © 2006 Elsevier B.V. All rights reserved.
doi:10.1016/j.sab.2006.09.014

wafer. The BioDot uses a high resolution syringe pump and a micro solenoid valve for droplet control and deposition. Each droplet was 20 nL of solution spaced 1 mm apart by the positioning software. The arrays were designed so that they would be within the analyzed area of the wafer based on the 80 mm^2 detector window of the TXRF. The solutions were 1% nitric acid (TamaPure, Kawasaki City, Japan) with various concentrations of Ni and Si (NIST, Gaithersburg, MD). The coordinates of the depositions were determined with a KLA-Tencor SP-1 or a Surfscan 6420 unpatterned surface inspection system (KLA-Tencor, San Jose, CA). All TXRF measurements were made with a Technos 630T instrument. The tungsten anode was operated at 30 kV and 200 mA with an incident angle of 0.12°, and the silver anode was operated at 40 kV and 35 mA with an incident angle of 0.06°. The atomic force microscopy (AFM) images were collected with a Digital Instruments Nanoscope III with Dimension 5000 multimode AFM in tapping mode. Auger analysis was carried out using a PHI 670 field emission instrument with a 10 keV and 10 nA electron beam.

3. Results and discussion

Typical deposition and drying times for various array sizes are shown in Table 1, along with total volume and mass for each array. Times reported are for both deposition and complete drying of the arrays at room temperature and pressure. Already it is clear that the automated deposition system has advantages over the manual deposition reported previously [12]. In almost the same amount of time (45 s) that it took the manual system to dry a 10 nL droplet, the automated system deposited and dried sixteen 20 nL droplets on the wafer (4×4 array). This may be due, in part, to desolvation of the droplet traveling from the tip of the BioDot to the wafer's surface. Fig. 1 shows the BioDot system depositing an array of 20 nL droplets onto a wafer. To show the feasibility of typical VPD volumes, 50 and 100 μL total volumes were also deposited on a wafer in a 10 mm by 10 mm area. For the 50 and 100 μL depositions, the time shown also includes waiting until the entire 10×10 array of 20 nL droplets was dry before beginning the next deposition; the droplets were spaced 0.1 mm away from the previous deposition area in the Y axis direction and 0.2 mm shifted in the X axis direction so that the droplet drying would be more influenced by the Si surface than contact with the other dried residues. A method such as heating the wafer would increase the sample throughput for these larger volumes by helping to dry the droplets more quickly.

Table 1
Average time for corresponding sized arrays of 20 nL droplets to be deposited and completely dried

Array size	Total volume nL	Total Ni mass ng	Time
3×3	180	1.8	35 s
4×4	320	3.2	44 s
5×5	500	5.0	52 s
10×10	2000	20.0	109 s
50 μL	50000	0.5	45 min
100 μL	100000	1.0	90 min

The 50 and 100 μL arrays were made up of series of 10×10 arrays (see text). All depositions were 10 μg/mL Ni except for the 50 and 100 μL depositions, which were 10 ng/mL Ni.

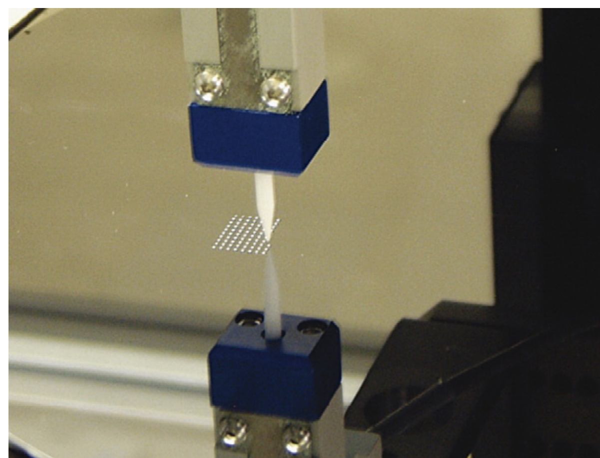

Fig. 1. Picture of a 10×10 array of 20 nL droplets being deposited on a bare Si wafer.

The coordinates of the arrays on the wafers were determined by one of the KLA-Tencor Surfscan unpatterned surface inspection systems. As the depositions were not done in a clean room, the arrays where the ambient particle background was too high to determine the exact coordinates by one of the Surfscans, the location of the array was calculated based on the spacing between arrays as prepared by the BioDot software and using the TXRF instrument's dropsearch software.

Fig. 2 shows representative angle scans of 3×3 arrays of 100 ng/mL (0.018 ng Ni) and 10 μg/mL (1.8 ng Ni) solutions using a W anode. These angle scans show the general trend of shifting away from a pure film-like response toward a residue-like response with an increase in concentration [13]. Nickel solutions that had an increase in matrix, for example Si in the solution, also showed the shift away from a pure film-like response. Similar behavior was observed with the angle scans of the Ag anode spectra. Fig. 3 shows AFM images of typical depositions of the 20 nL droplet from the 3×3 arrays of the 10 μg/mL Ni solution. There were a total of twenty-seven 20 nL droplets from the 3×3 arrays (three replicates were deposited).

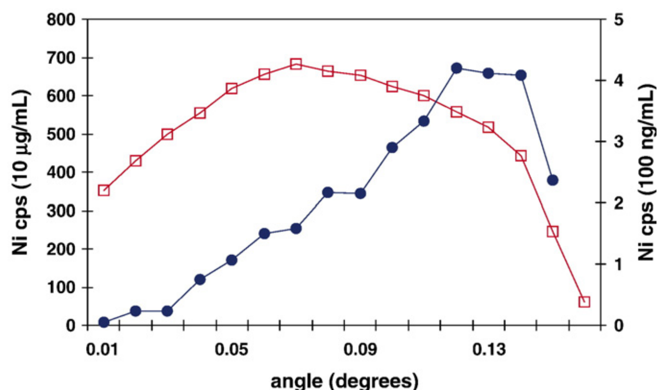

Fig. 2. Representative angle scans of 3×3 arrays of 100 ng/mL (closed circles) and 10 μg/mL (open squares) Ni solutions.

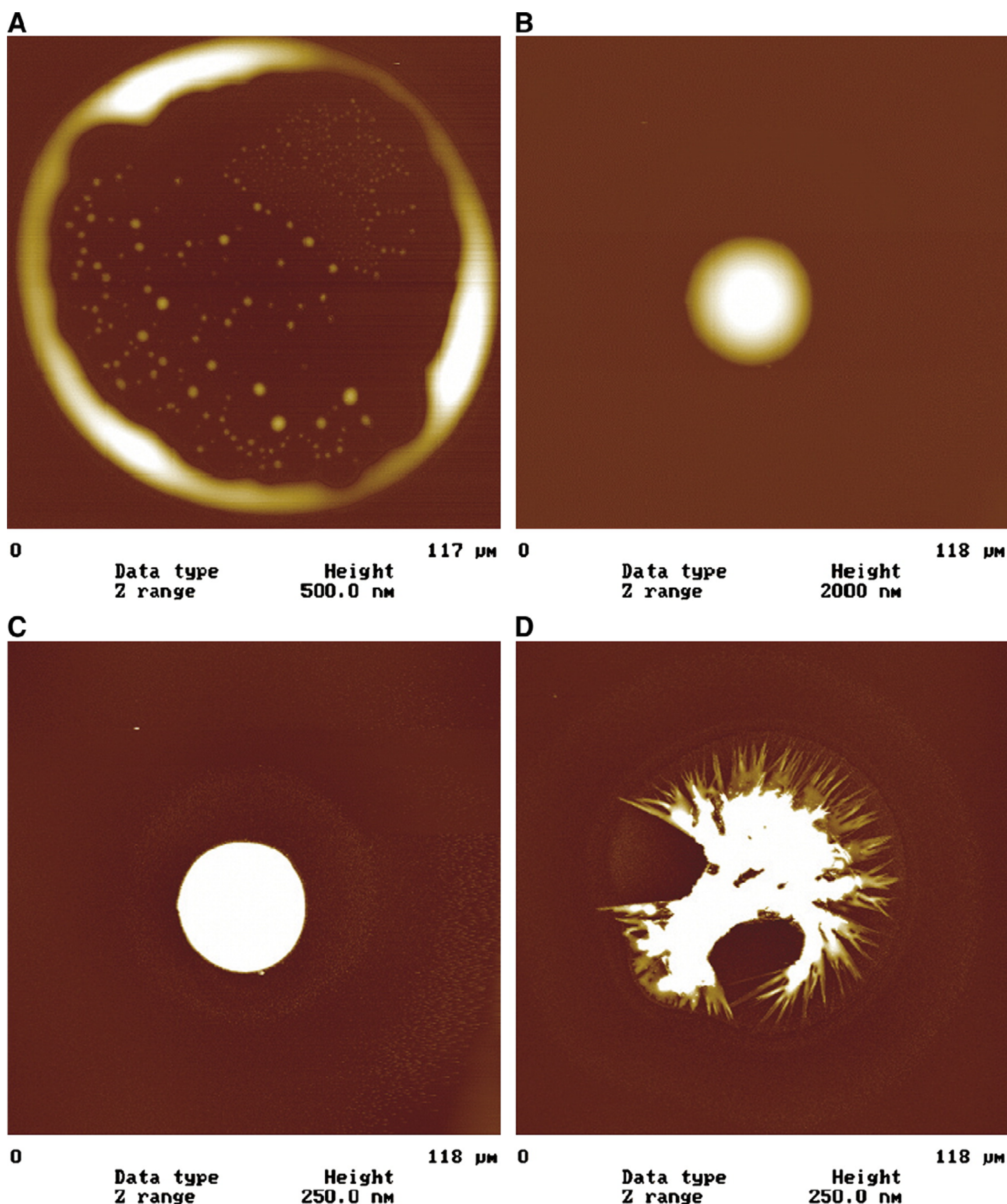

Fig. 3. AFM images of dried residues of 20 nL of 10 µg/mL Ni solution. (A) shows a ring shaped residue with a *z* scale of 500 nm, (B) and (C) images show the same well-defined droplet with *z* scales of 2000 nm (B) and 250 nm (C), (D) shows a crystallized residue with a *z* scale of 250 nm.

Of these, about 70% of the droplets dried in the ring-like structure (Fig. 3A) and about 15% dried in the smaller, well-defined droplet structure (Fig. 3B and C). The other droplets dried in a mixture between the two or a crystallized structure (e.g., Fig. 3D). The ring-like dried spots were about 100–120 µm in diameter; the brighter areas indicate greater intensity of the *z*-axis (coming out of the page). The height of the dried droplet was about 500 nm around the edges of the ring. The well-defined droplets dried in spots that were 30–40 µm in diameter with a *z*-axis height of 2000 nm. A close look at Fig. 3C shows a smaller *z*-axis scale than Fig. 3B with concentric rings around the well-defined droplet at a lower *z* height as if it had dried leaving some residue behind in the rings; however, the majority of the residue was in the well-defined droplet. A similar analysis of a more concentrated Ni deposition solution (100 µg/mL) shows the majority of the depositions were in the category of a well-defined droplet and no ring-like dried spots. The formation of more of the taller, in the *z*-axis direction, well-defined droplets with increasing Ni concentration may be a factor in the shape of the angle scan curves

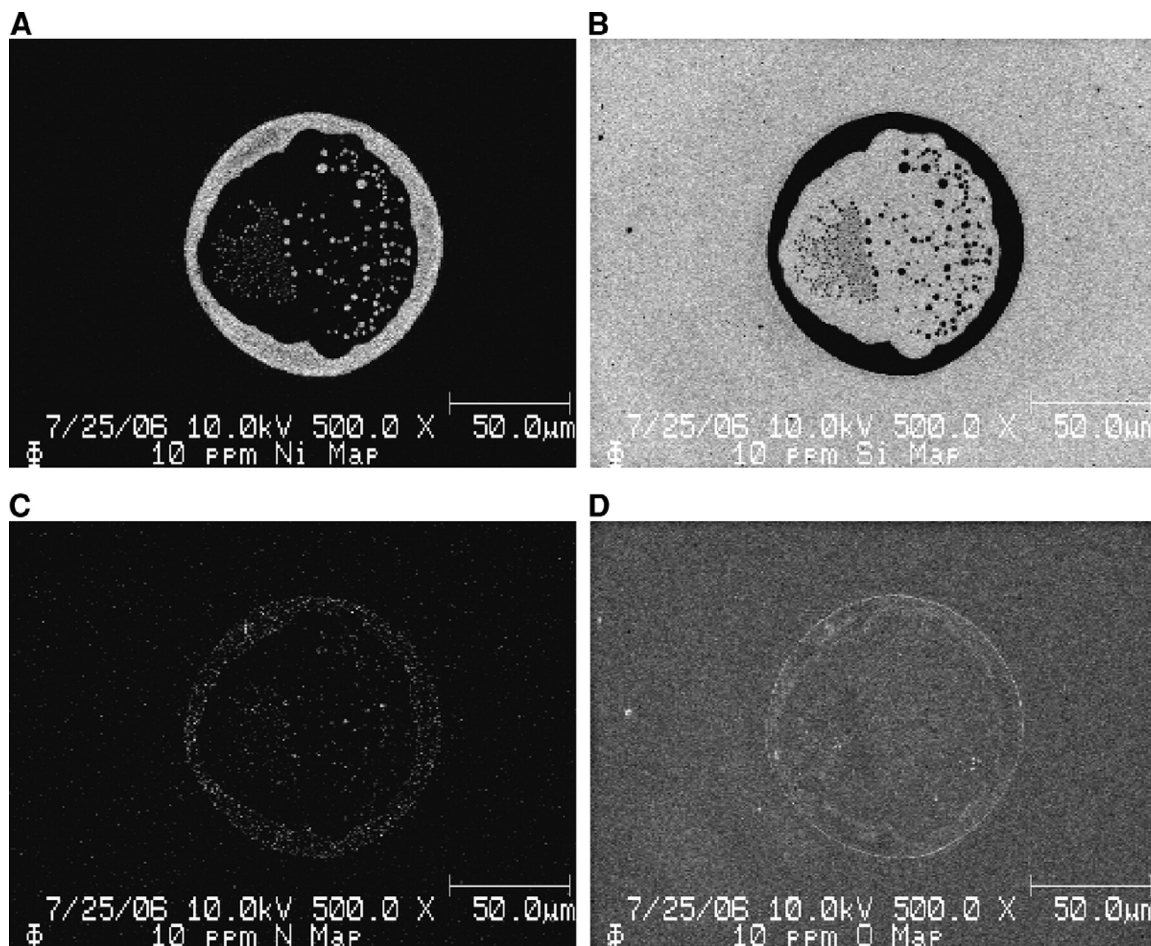

Fig. 4. Auger element maps of a ring shaped 20 nL residue of 10 µg/mL Ni solution. The brighter areas indicate a more intense signal. (A) shows the Ni map, (B) shows the Si map, (C) shows the N map, and (D) shows the O map.

transitioning from film-like to residue-like formations. Parameters such as distance to surface, solenoid opening duration, and chamber humidity may affect the dried residue formation. These parameters will be studied in future experimental work.

The dried residues were also characterized with Auger electron spectroscopy. Element maps from the Auger of a 20 nL droplet of 10 µg/mL Ni are shown in Fig. 4, similar to the residue shown in Fig. 3A. Brightness in the image indicates a more intense signal. Fig. 4A shows the majority of the Ni is contained in the ring structure with some residual Ni in the center. By contrast, there is no Si signal (Fig. 4B) detected in the ring structure indicating that the Ni residue layer is thick enough to block the escape of Si Auger electrons from the substrate. Fig. 4C and D shows respectively the N and O element maps. As the Ni was prepared in a nitric acid solution, the evident ring patterns for N and O may imply that the Ni dries as a nitrate salt. Element maps from the Auger were also collected on a well-defined droplet like the one shown in Fig. 3B. In this case, there was too much charging on the sample to get a map for Ni, but the Si map again showed complete blockage of the silicon signal in the area of the well-defined droplet.

To test the linearity of the TXRF signal with individual droplets, Fig. 5 plots the relationship between the number of droplets deposited and the signal from the TXRF for both the W and the Ag anodes. The droplets were each 20 nL of 1 µg/mL Ni (the average in Fig. 5 is for a replicate of $n=2$ for 1, 2, 4, 6, and 8 droplets). Both anodes show a similar linear response to the number of droplets deposited. Angle scans with both the W and Ag anodes showed mostly a film-like response to the individual droplet deposition.

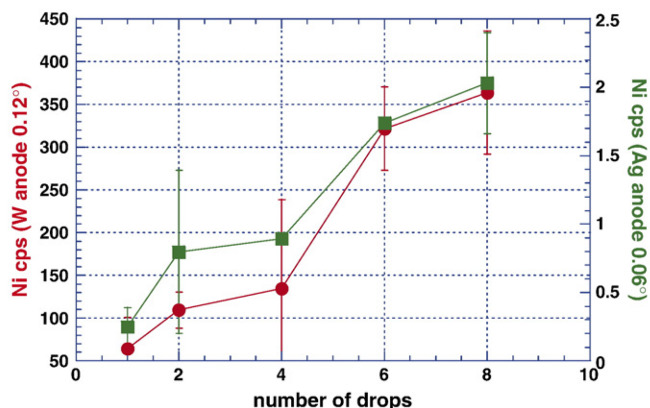

Fig. 5. Relationship between the TXRF signal for the W anode (circles) and the Ag anode (squares) versus the number of 20 nL droplets of 1 µg/mL Ni solution ($n=2$).

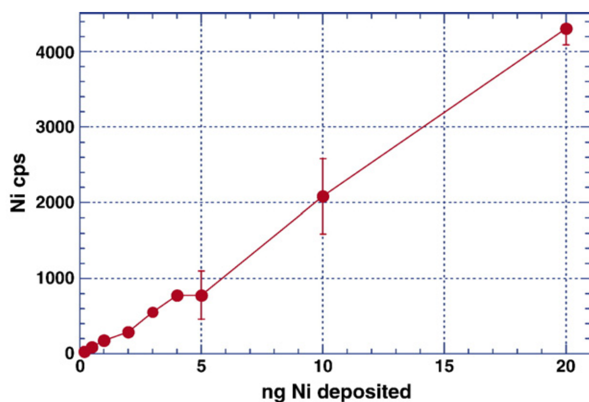

Fig. 6. Nanograms of Ni deposited in 10×10 arrays of 20 nL droplets versus TXRF signal using the W anode at 0.12° (n=2, R^2=0.995).

Recent literature has shown that the linearity of the TXRF signal of a VPD residue ends around 3 ng [5,6], but for a corresponding concentration in a film-like (spun on) sample the linearity is extended [11]. By taking advantage of the programming capability of the BioDot deposition, such that the VPD residue was distributed evenly within the analysis area of the TXRF detector, the linearity could be extended beyond 3 ng. In Fig. 6, 0.2 ng to 20 ng of Ni are deposited on a wafer in sets of 10×10 arrays (n=2). Each of the 20 nL droplets is spaced 1 mm apart for a 9 mm×9 mm array (with a 12.7 mm diagonal). The 80 mm^2 window of the detector on the TXRF has a diameter of 10 mm; therefore, the Ni solution is evenly spread over the area viewed by the detector except for the area in the corners where the square array slightly extends from the circular detector analysis area. A linear response up to 20 ng of deposited Ni is seen in Fig. 6. This is almost an order of magnitude greater than previously reported for normal VPD type residues dried on a wafer. The error bars of the last three points (5, 10, and 20 ng of Ni) are greater than those for the first six data points. There are possibly two explanations for this.

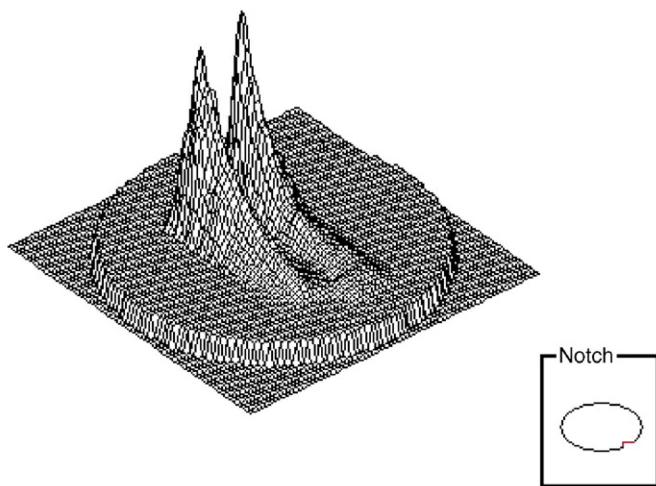

Fig. 7. A 3-dimensional view where the z-axis is Ni signal intensity measured by TXRF mapping. There are two side by side 10×10 arrays deposited on a silicon wafer with the total Ni concentration of the array increasing from 0.2 ng (lower right) to 4 ng (upper left).

Table 2
Precision of the Ni intensity compared to array size and total mass of Ni deposited (n=3)

Array size	Concentration of Ni deposited	Ni mass deposited (ng)	Ni intensity (cps)	% RSD
5×5	10 μg/mL	5	1323±170	12.8
4×4	10 μg/mL	3.2	745±245	32.9
3×3	100 μg/mL	18	4205±122	2.9
3×3	10 μg/mL	1.8	514±30.0	5.8
3×3	1 μg/mL	0.18	25.8±11.7	45.3
3×3	100 ng/mL	0.018	4.06±0.59	14.5
3×3	blank	0	0	

Due to spacing considerations, the arrays were deposited on two wafers which came from different lots with the last three sets of arrays (5, 10, and 20 ng of Ni) deposited on a wafer different from that which had the first six sets of arrays, thus the surfaces of the wafers may have been slightly different allowing for different droplet drying conditions. Also there may be different types of residue shapes left on the wafer, as seen in Fig. 3, with increasing concentrations of Ni solutions. Angle scans of these depositions also showed the trend of a film-like response for the lower concentrations which transitioned into a mixture of film-like and residue response for the highest concentrations. Taking advantage of a recent upgrade to the TXRF which enables contamination mapping, Fig. 7 shows a 3-dimensional wafer map of the Ni counts on the surface of the wafer having side by side arrays of 0.2 to 4 ng of Ni deposited on it. The notch end of the wafer, as indicated by the chart on the lower right, had the 0.2 ng depositions and a low Ni signal intensity. Concentration of Ni deposited on the wafer increased, moving across the wafer away from the notch and likewise so did the Ni signal intensity. Two-hundred points were measured on the wafer at 30 s each in the mapping mode of the TXRF. The side by side depositions of the arrays with increasing intensity are easily distinguished in this figure.

Along with determining the extent of the linearity of the TXRF signal using the nanoliter depositions, the reproducibility of the depositions was also studied. Table 2 lists the array size, concentration of Ni solution deposited, total mass of Ni

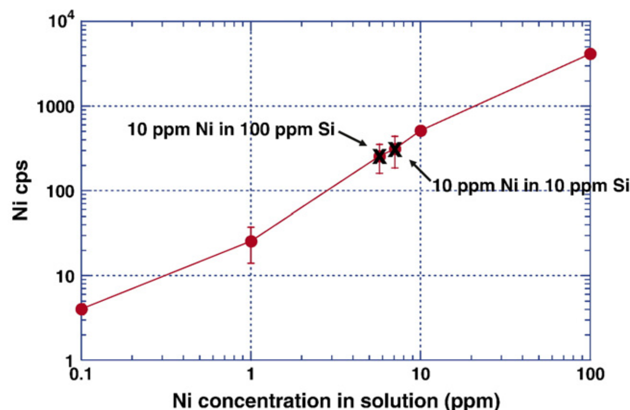

Fig. 8. Calibration curve of 3×3 arrays of Ni solution deposited on a wafer showing the effect of adding 10 μg/mL and 100 μg/mL of Si to the matrix (n=3).

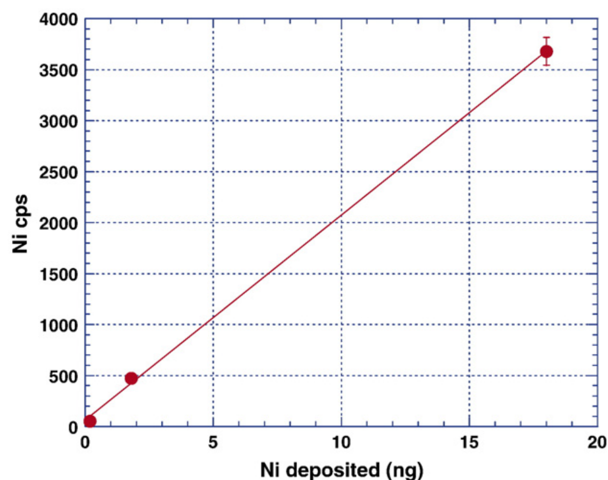

Fig. 9. TXRF signal from 3 × 3 arrays of Ni deposited on a wafer with a Ru film substrate (n = 3).

deposited, intensities, and relative standard deviations (n = 3). The precision of the TXRF signal varied from 3 to 45%. There was no clear correlation between better precision and array size or mass deposited, although higher concentrations of Ni tended to have better precision. The previously reported manual deposition of single droplets of 10 nL had 3 to 6% RSDs for concentrations of 0.05 to 0.5 ng [12].

As an example of an application of the nanoliter deposition, Fig. 8 plots a calibration curve constructed with 3 × 3 arrays of increasing concentrations of Ni (n = 3). Also plotted on the calibration curve are averages of the Ni signal intensities of 3 × 3 arrays of 10 μg/mL Ni in either 10 μg/mL Si or 100 μg/mL Si solution to simulate a VPD type matrix (n = 3). From this figure, it is clear that even with nanoliter quantities of solution, additional matrices suppress the analyte signal. In this case, the 10 and 100 μg/mL Si matrix caused a signal suppression of 29 and 43%, respectively, when there was 10 μg/mL of Ni in the solution deposited. Angle scans from the 10 μg/mL Ni, the10 μg/mL Ni with 10 μg/mL Si, and the 10 μg/mL Ni with 100 μg/mL Si all showed similar profiles, mostly film-like with a transition towards residue-like formations with increasing Si content.

As the TXRF is being used to characterize the new films being introduced into the semiconductor process line and to monitor for cross contamination from these new materials [14–18], nanoliter depositions can be used with TXRF to improve upon the characterization process. Fig. 9 shows a calibration curve of 3 × 3 arrays of nanoliter depositions of 0.18 ng, 1.8 ng, and 18 ng of Ni (n = 3) on a 1000 Å Ru film using the W anode for analysis. By demonstrating good linearity (R^2 = 0.9994) on a non-Si surface, the nanoliter depositions were used to create a working standard for contamination on a Ru film. This indicates that the method should be capable of being extended to other new materials being introduced into semiconductor processing.

4. Conclusions

The BioDot system is an effective method of depositing arrays of sample onto a Si wafer, implying that a more optimized deposition system would be promising for VPD measurements. Throughput was significantly improved over the manual deposition system. Further improvements to deposition throughput could be achieved by driving off the matrix solution with heat or a system such as the piezoelectric ink jet capable of dispensing smaller volumes, which would dry more rapidly, increasing throughput and generating potentially smaller residues with increased reproducibility.

By taking advantage of the BioDot's programmable arrays and spreading the deposition out completely under the analysis area of the TXRF's detector, the linearity of the TXRF response to a deposition can be increased from what has been previously reported. Linearity up to 20 ng of deposited Ni is shown, almost an order of magnitude higher than standard depositions. Theoretical calculations suggest this could be extended another order of magnitude [11].

As VPD and TXRF are moving to a higher level of automation [19–21], incorporating some type of nanoliter, or smaller volume, deposition process should be a feasible and more reproducible alternative to the current methodologies that use temperature and pressure to control the analyte drying on the wafer.

Acknowledgements

CMS would like to thank Meredith Beebe and Dale Sheu of ATDF for their assistance with the particle counters and location of the arrays on the wafers.

References

[1] International Technology Roadmap for Semiconductors, http://public.itrs.net.

[2] G. Buhrer, Application of vapor phase decomposition/total reflection X-ray fluorescence in the silicon semiconductor manufacturing environment, Spectrochim. Acta Part B 54 (1999) 1399–1407.

[3] A. Huber, H. Rath, P. Eichinger, Th. Bauer, L. Kotz, R. Staudigl, Sub-ppm monitoring of transition metal contamination on silicon wafer surfaces by VPD-TXRF, Electrochem. Soc. Proc. 88–20 (1988) 109–112.

[4] C. Neumann, P. Eichinger, Ultra-trace analysis of metallic contaminations on silicon wafer surfaces by vapour phase decomposition/total reflection X-ray fluorescence (VPD/TXRF), Spectrochim. Acta Part B 46 (1991) 1369–1377.

[5] D. Hellin, W. Fyen, J. Rip, T. Dalande, P. Mertens, S. De Gendt, C. Vinckier, Saturation effects in TXRF on micro-droplet residue samples, J. Anal. At. Spectrom. 19 (2004) 1517–1523.

[6] D. Hellin, J. Rip, S. Arnauts, S. De Gendt, P. Mertens, C. Vinckier, Validation of vapor phase decomposition-droplet collection-total reflection X-ray fluorescence spectrometry for metallic contamination analysis of silicon wafers, Spectrochim. Acta Part B 59 (2004) 1149–1157.

[7] R. Hockett, J. Metz, S. Tan, Quantification issues for VPD/TXRF, Proceedings of the Second International Symposium on Ultra-Clean Processing of Silicon Surfaces, (1994) pp. 171–175.

[8] N. Alov, K. Oskolok, A. Wittershagen, B. Kolbesen, TXRF characterization of inhomogeneous solids: influence of surface morphology, Electrochem. Soc. Proc. 2003–03 (2003) 129–135.

[9] L. Fabry, S. Pahlke, L. Kotz, Accurate calibration of TXRF using microdroplet samples, Fresenius J. Anal. Chem. 345 (1996) 266–270.

[10] C. Streli, G. Pepponi, P. Wobrauschek, N. Zöger, P. Pianetta, K. Baur, S. Pahlke, L. Fabry, C. Mantler, B. Kanngießer, W. Malzer, Analysis of low Z elements on Si wafer surfaces with synchrotron radiation induced total reflection X-ray fluorescence at SSRL, Beamline 3-3: comparison of droplets with spin coated wafers, Spectrochim. Acta Part B 58 (2003) 2105–2112.

[11] D. Hellin, J. Rip, V. Geens, T. Delande, T. Conard, S. De Gendt, C. Vinckier, Remediation for TXRF saturation effects on microdroplet residues from preconcentration methods on semiconductor wafers, J. Anal. At. Spectrom. 20 (2005) 652–658.

[12] T. Miller, C. Sparks, G. Havrilla, M. Beebe, Semiconductor applications of nanoliter droplet methodology with total reflection X-ray fluorescence analysis, Spectrochim. Acta Part B 59 (2004) 1117–1124.

[13] R. Klockenkämper, Total Reflection X-ray Fluorescence Analysis, John Wiley & Sons, New York, 1997, p. 192.

[14] C. Sparks, M. Beebe, J. Bennett, B. Foran, C. Gondran, A. Hou, Characterization of high-*k* gate dielectric and metal gate electrode semiconductor samples with a total reflection X-ray fluorescence spectrometer, Spectrochim. Acta Part B 59 (2004) 1227–1234.

[15] D. Hellin, A. Delabie, R. Puurunen, P. Beaven, T. Conard, B. Brijs, S. De Gendt, C. Vinckier, Grazing incident X-ray fluorescence spectrometry for the compositional analysis of nanometer thin high-*k* dielectric HfO_2 layers, Anal. Sci. 21 (2005) 845–850.

[16] D. Hellin, B. Onsia, A. Delabie, S. DeGendt, C. Vinckier, The role of TXRF in the introduction of high-k materials into IC processing, Electrochem. Soc. Proc. 2003–22 (2003) 199–211.

[17] D. Hellin, V. Geens, I. Teerlinck, J. Van Steenbergen, J. Rip, W. Laureyn, G. Raskin, P. Mertens, S. De Gendt, C. Vinckier, Vapor phase decomposition-droplet collection-total reflection X-ray fluorescence spectrometry for metallic contamination analysis on Ge wafer, Spectrochim. Acta Part B 60 (2005) 209–213.

[18] C. Sparks, P. Lysaght, T. Rhoad, Measurement of the silicon dioxide concentration in hafnium silicate gate dielectrics with a TXRF, Powder Diffr. 20 (2005) 161–164.

[19] A. Huber, F. Freudenberg, Fully automatic wafer surface contamination monitoring based on VPD-TXRF, Electrochem. Soc. Proc. 99–16 (1999) 221–231.

[20] M. Yamagami, A. Ikeshita, Y. Onizuka, S. Kojima, T. Yamada, Development of vapor phase decomposition-total-reflection X-ray fluorescence spectrometer, Spectrochim. Acta Part B 58 (2003) 2079–2084.

[21] Y. Mori, K. Uemura, M. Yamagami, T. Yamada, A method of locating dried residue on a semiconductor wafer in vapor phase decomposition-total-reflection X-ray fluorescence spectrometry by monitoring scattered X-rays, Spectrochim. Acta Part B 56 (2001) 2293–2300.